Alternative Splicing of Human Insulin-Degrading Enzyme Yields a Novel Isoform with a Decreased Ability To Degrade Insulin and Amyloid β-Protein†

Wesley Farris, Malcolm A. Leissring, Matthew L. Hemming, Alice Y. Chang, and Dennis J. Selkoe*

Center for Neurologic Diseases, Department of Neurology, Brigham and Women's Hospital, Harvard Medical School, Boston, Massachusetts 02115

Received November 3, 2004; Revised Manuscript Received February 7, 2005

ABSTRACT: Deletion of insulin-degrading enzyme (IDE) in mice causes accumulation of cerebral amyloid β-protein (Aβ), hyperinsulinemia, and glucose intolerance. Together with genetic linkage and allelic association of IDE to Alzheimer's disease (AD) and type 2 diabetes mellitus (DM2), these findings suggest that IDE hypofunction could mediate human disease. To date, no coding mutations have been found in the canonical isoform of IDE, suggesting that pathological mutations could exist in undiscovered exons or regulatory regions, including untranslated regions (UTRs). However, neither isoforms arising from alternative splicing nor the UTRs have been described. Here, we systematically characterize human IDE mRNAs, identify a novel splice form, and compare its subcellular distribution, kinetic properties, and ability to degrade Aβ to the known isoform. Six distinct human IDE transcripts were identified, with most of the variance attributable to alternative polyadenylation sites. In the novel spliceoform, an exon we designate "15b" replaces the canonical exon "15a", and the resultant variant is widely expressed. Subcellular fractionation, immunofluorescent confocal microscopy, and immunogold-electron microscopy reveal that the 15b-IDE protein occurs in both cytosol and mitochondria. Organelle targeting of both isoforms is determined by which of two translation start sites is used, and only those isoforms utilizing the second site regulate levels of secreted Aβ. 15b-IDE can exist as a heterodimer with the 15a isoform or as a homodimer. The apparent K_m values of recombinant 15b-IDE for both insulin and Aβ are significantly higher and the k_{cat} and catalytic efficiency markedly lower than those of 15a-IDE. In accord, cells coexpressing β-amyloid precursor protein (APP) and 15b-IDE accumulated significantly more Aβ in their media than those expressing APP and 15a-IDE. Our results identify a novel, catalytically inefficient form of IDE expressed in brain and non-neural tissues and recommend novel regions of the IDE gene in which to search for mutations predisposing patients to AD and DM2.

Insulin-degrading enzyme (IDE,[1] insulysin, EC 3.4.24.56) is an ∼110 kDa member of the M16 ("inverzincin") family of zinc metalloproteases, characterized by the presence of the HXXEH catalytic site motif, which is inverted relative to the more common HEXXH catalytic site of zinc metalloproteases. IDE is located primarily within the cytosol but has also been detected in endosomes, in peroxisomes, on the cell surface (*1*), and most recently in mitochondria (*2*). The protease has been shown to cleave several small proteins of diverse sequence in vitro, including insulin, amyloid β-protein (Aβ), glucagon, insulin-like growth factor II, amylin, β-endorphin, atrial natriuretic peptide, transforming growth factor α, and the intracellular domain of APP (AICD) (*1*, *3*, *4*). Homozygous deletion of the IDE gene in mice results in an up to ∼65% increase in the levels of brain Aβ, an ∼180% increase in serum insulin levels, and impaired glucose tolerance (*5*, *6*). Thus, selective deletion of IDE in vivo recapitulates some of the hallmark phenotypic characteristics of Alzheimer's disease (AD) (chronic elevation of cerebral Aβ levels) and of type 2 diabetes mellitus (DM2) (hyperinsulinemia and glucose intolerance). Moreover, naturally occurring partial loss-of-function mutations in IDE that are sufficient to induce a diabetic phenotype in the rat also result in impaired neuronal Aβ catabolism (*7*).

In human genetic studies, the IDE region of chromosome 10q has shown linkage to late-onset AD (*8*), DM2 (*9*, *10*), and fasting plasma glucose levels (*11*). Allelic association within or very near the IDE gene has also been reported with late-onset AD (*8*, *12*−*15*); the AD-related quantitative traits of mini-mental state exam scores, degree of brain pathology, age of onset (*14*), and plasma $Aβ_{42}$ levels (*16*); DM2 (*17*); and the DM2-related quantitative traits of hemoglobin A_{1c} levels, fasting plasma glucose levels (*17*), and plasma insulin levels (*18*). However, studies in other populations have found

† This work was supported by NIH Grants NS046324 and AG12749 and by the Foundation for Neurologic Diseases.

* To whom correspondence should be addressed: HIM 730, 77 Ave. Louis Pasteur, Boston, MA 02115. Telephone: (617) 525-5200. Fax: (617) 525-5252. E-mail: dselkoe@rics.bwh.harvard.edu.

[1] Abbreviations: IDE, insulin-degrading enzyme; Aβ, amyloid-β protein; AD, Alzheimer's disease; DM2, type 2 diabetes mellitus; UTR, untranslated region of mRNA; APP, β-amyloid precursor protein; AICD, APP intracellular domain; NCBI, National Center for Biotechnology Information; FLJ, full-length long Japan genome project; RLM-RACE, RNA ligase-mediated rapid amplification of cDNA ends; HA, hemagglutinin; CHO, Chinese hamster ovary; VDAC, voltage-dependent anion channel; PAGE, polyacrylamide gel electrophoresis; GST, glutathione *S*-transferase; ELISA, enzyme-linked immunosorbant assay; CNS, central nervous system.

10.1021/bi0476578 CCC: $30.25
Published on Web 04/07/2005

no allelic association of IDE with AD (*19*−*21*) or DM2 (*22*). Taken together, the available genetic evidence and the aforementioned functional data in living animals suggest that IDE hypofunction could have a role in two major diseases and provide a potential mechanism for the recently recognized epidemiological association among hyperinsulinemia, DM2 and AD (*23*−*29*).

Despite the growing body of genetic data implicating IDE in disease, none of the single-nucleotide polymorphisms examined in the coding regions of the well-characterized 25-exon canonical form of IDE [National Center for Biotechnology Information (NCBI) entry NM_004969] appears to be a pathological mutation. This realization suggests that if such mutations exist, they may occur in novel exons, the regulatory elements found in UTRs of transcripts, or untranscribed regulatory regions (e.g., promoters, enhancers, and repressors). No protein isoforms from alternative splicing have been described, although we recently found that the subcellular localization of the known 25-exon IDE is determined in part by which of two potential translation start sites is used (*2*). Rat and *Drosophila* have two IDE transcripts (~3.5 and ~6 kb) with a wide tissue distribution, and rats have two additional transcripts (~4 and ~6.5 kb) exclusively in the testis (*30*−*32*). Two different-sized IDE mRNAs (~3.1 and ~3.5 kb) have also been noted in human hepatoma and lymphoblast cell lines (*33*). The nature of these different mRNAs has not been investigated. In addition to the well-known 25-exon form of human IDE, there is a truncated IDE transcript in the NCBI database (AK093287) that was directly submitted by the full-length long Japan (FLJ) human cDNA sequencing project (*34*). This ~1.9 kb transcript, found only in testis, lacks the typical exons 1−11 and 15 (and thus the protease's catalytic site in exon 3) and contains two novel exons. Little else is known about IDE mRNAs.

The goal of this study was to obtain a better understanding of human IDE transcripts and to discover and characterize any natural IDE variants that may exist. We were specifically interested in characterizing the UTRs and novel isoforms containing the catalytic site so that we could both obtain a better understanding of the normal biology of this important protease and identify new sequences that could harbor the elusive pathological mutations in the AD or DM2 subjects in whom IDE has been genetically implicated. Furthermore, we hypothesized that if natural variants of IDE exist, they may possess altered degradative capacity, a finding which could have relevance for the potential role of the protease in DM2 or AD. We systematically characterized the number, size, tissue distribution, and UTRs of human IDE transcripts, and we identified a novel splice variant. This novel spliceoform was then cloned from two disease-relevant tissues: brain, where Aβ accumulates in AD, and liver, the major organ for insulin clearance (*1*). The two IDE splice variants were expressed in cultured cells, either in wild-type form or as variants translated obligatorily from the first or second initiation codon, and we then compared their subcellular localization, ability to form homodimers and heterodimers, and degradative capacity on endogenously produced Aβ. We also generated recombinant forms of the two splice variants and compared their detailed kinetic properties, using both Aβ and insulin as substrates.

EXPERIMENTAL PROCEDURES

Northern Blotting. Probe templates were amplified from a human liver cDNA library (Ambion), gel purified, sequenced, and then used in a linear PCR with [^{32}P]dATP and the antisense primer. Northern Human Blot 2 (Ambion), Human 12-Lane Multiple Tissue Blot (Clontech), and Human Brain Blot II (Clontech) were each prehybridized and hybridized in ULTRAhyb buffer (Ambion) at 42 °C, and washed for a total of 45 min at 42 °C with NorthernMax Low and High Stringency washes (Ambion). Signals were detected by autoradiography using either BioMax MS film (Kodak) together with an intensifying screen or a PhosphorImager screen (Molecular Dynamics).

RNA Ligase-Mediated Rapid Amplification of cDNA Ends (RLM-RACE). Nested PCR was performed on RACE-Ready cDNA (Ambion) per the manufacturer's instructions. RACE products were gel purified and sequenced.

Cloning and Expression of Splice Variants. 15b-containing IDE was selectively amplified from a liver cDNA library by PCR using two sets of primers chosen so that the two amplicons overlapped only by exon 15b. The two fragments were digested with a 15b-specific restriction endonuclease (BstZ17I), ligated to form the entire 15b-IDE coding sequence, inserted into the pCR2.1 TOPO vector (Invitrogen), and sequenced. By restriction digestion and ligation, we replaced exon 15a with exon 15b in the three previously generated (*2*) hemagglutinin (HA)-tagged human IDE-pcDNA5/FRT expression vectors with translation beginning obligatorily at Met1 due to a Met42 mutation to Ala (Met1-IDE), obligatorily at Met42 due to removal of the Met1 codon (Met42-IDE), or at either Met (wt-IDE). The internal HA tag immediately followed Arg43, and a Kozak consensus sequence was placed before Met1 in the Met1-HA-IDE constructs to improve expression. As previously described for the canonical 15a-containing constructs (*2*), we generated CHO cell lines stably expressing each of the three 15b-containing constructs utilizing Invitrogen's Flp-In system. This allowed stable integration of each construct into the same genomic locus of a single cell line. Transient transfections were performed using either Lipofectamine 2000 (Invitrogen) or GenePorter 2 (GTS), and expression of the constructs was assayed 32−48 h after transfection.

Subcellular Fractionation. Intact cells were dissociated from a confluent monolayer with 5 mM EDTA in PBS, and mitochondrial fractions were prepared as described previously (*2*). However, in the current work, the postnuclear supernatant underwent subsequent spins at 5000*g* for 10 min, 12000*g* for 10 min, and 100000*g* for 1 h to generate three pellet fractions containing intact organelles and a cytosol fraction. After being washed in isotonic lysis buffer, each pellet was divided into three equal parts. One part was washed with 10 mM HEPES/1× Hanks' Balanced Salt Solution (HBSS) (pH 7.4) to preserve organelle integrity; another part was washed twice with 100 mM Na_2CO_3 (pH 11.3) with 10 s of sonication during each wash, and the third part was washed first with Na_2CO_3 followed by 2 M urea with 10 s of sonication during each wash. After each sonication and wash, pellets were spun at 100000*g* and the supernatants were discarded to selectively retain membrane-bound protein. All pellets were ultimately resuspended in 50 mM Tris-HCl containing protease inhibitors and 1% SDS.

Samples were then analyzed by SDS−polyacrylamide gel electrophoresis (PAGE) and immunoblotting with antibodies against IDE [IDE-1 (*35*)], HA tag (3F10, Roche), Hsp60 (Stressgen), voltage-dependent anion channel (VDAC) (PA1−954, Affinity BioReagents), and catalase (Rockland).

Immunofluorescence Confocal Microscopy and Immunogold-Electron Microscopy. For confocal microscopy, the stably transfected CHO cells were plated onto 15 mm glass coverslips (coated with poly-D-lysine, poly-L-lysine, and laminin), fixed with 4% paraformaldehyde, and washed with PBS. The cells were permeabilized with 0.25% Triton X-100 and 0.5% DMSO, blocked with 10% normal goat serum, and then incubated in 3% BSA/PBS with primary antibodies against the HA tag (3F10), cytochrome *c* (6H2.B4, BD PharMingen), or catalase. After being washed, cells treated with the 3F10 antibody were incubated with biotinylated anti-rat IgG (Vector Laboratories) and then incubated with the streptavidin−Alexa Fluor 488 conjugate (Molecular Probes), whereas cells treated with the 6H2.B4 or anti-catalase antibodies were incubated with the appropriate secondary antibody conjugated to Alexa Fluor 594 (Molecular Probes). Visualization was accomplished using the 100× oil-immersion objective of a Zeiss 510 laser scanning microscope. Immunogold-electron microscopy was performed as previously described (*2*).

Immunoprecipitation and Immunoblotting. A C-terminally V5-tagged human 15a-wt-IDE construct in pEF6/V5-His-TOPO (Invitrogen) was transiently coexpressed in CHO cells with either the HA-tagged 15a- or 15b-wt-IDE construct described above. As controls, all three constructs were also transfected alone into CHO cells. The cells were lysed in 50 mM Tris-HCl, 150 mM NaCl, 1% NP-40, and a protease inhibitor cocktail (Roche) (pH 7.4), and protein concentrations were determined using a bicinchoninic acid-based assay (Pierce). After equal amounts of protein from each lysate were incubated with an anti-HA affinity matrix (Roche) on a nutator at 4 °C for 10 h, the matrix was washed thrice with fresh lysis buffer and boiled in SDS sample buffer. The matrix was pelleted, and SDS−PAGE and immunoblotting with an anti-V5 antibody (Invitrogen) were performed on the supernates. Blue-native gel electrophoresis was performed as previously described (*36*).

Generation and Purification of Recombinant IDE. To generate bacterial expression constructs encoding N-terminally tagged glutathione *S*-transferase (GST)−IDE fusion proteins, the sequence encoding human 15a-Met42-IDE from the pcDNA5/FRT expression vector described above was subcloned into pGex-6p-1 (Amersham Biosciences). GST-tagged 15b-Met42-IDE was generated by insertion of a BamHI−EcoRI fragment containing exon 15b derived from the 15b-Met42-IDE pcDNA5/FRT vector. The resulting constructs were used to transform the Rosetta strain of *Escherichia coli* (Novagen), and protein expression was induced by 50 μM IPTG, followed by incubation for 16 h at 27 °C. Bacterial pellets were resuspended in PBS with 1 mM DTT and protease inhibitor cocktail without EDTA (Roche), and were lysed by two passages through a French pressure cell (SLM-Aminco) at 1000 psi. Insoluble proteins and cellular debris were removed by centrifugation at 20000*g* for 10 min. The supernate was applied to a glutathione−Sepharose column (Amersham Biosciences) and washed extensively with PBS/1 mM DTT. The recombinant IDE protein was released from the column by cleavage of the GST tag with PreScission protease (Amersham Biosciences) according to manufacturer's recommendations.

Degradation Assays. Insulin and Aβ_{40} degradation assays were carried out by trichloroacetic acid precipitation assays as described previously (*5*). Kinetic data were obtained by incubating the recombinant enzyme (1.1 and 11 nM for 15a- and 15b-IDE, respectively) with different amounts of unlabeled recombinant human insulin (Sigma) or synthetic Aβ_{40} (generated in-house through automated fluoren-9-ylmethoxycarbonyl chemistry) supplemented with 100 pM recombinant human [^{125}I]insulin and [^{125}I]Aβ_{40} (Amersham Pharmacia), respectively. Reactions were carried out in duplicate at 37 °C in 50 mM HEPES (pH 7.4), 100 mM NaCl, and 10 mM $MgCl_2$, supplemented with 0.1% bovine serum albumin, and incubation times were adjusted to achieve ∼5−10% cleavage of the iodinated peptide. Kinetic parameters were calculated by hyperbolic regression analysis as previously described (*37*).

Quantification of Aβ in Conditioned Media. Transient transfections of CHO cells stably expressing human β-amyloid precursor protein $(APP)_{751}$ containing the V717F AD-causing missense mutation, collection of conditioned media, and measurement of Aβ X-40 and X-42 levels by an enzyme-linked immunosorbant assay (ELISA) were performed as previously described (*5*, *38*).

RESULTS

Four Variants of IDE mRNA Contain the Catalytic Site Sequence and Are Widely Distributed. Tissue-specific expression of the human IDE gene was first examined by Northern blot analysis using a probe against the catalytic site sequence in exon 3 and adjoining sequence in exon 2. The 316 bp probe detected IDE mRNA in each of the 15 tissues examined on two distinct multiple-tissue Northern blots and in eight different regions of the human central nervous system (CNS) (Figure 1A). After prolonged exposure, four different transcripts could be visualized in 12 of the tissues and all regions of the CNS, whereas heart, lung, and leukocytes lacked the largest transcript. The sizes of corresponding mRNAs from each blot were estimated, and the two values were averaged to give estimated transcript sizes of 3.5, 3.8, 5.5, and 9 kb. The ∼5.5 kb transcript was the predominant species in every tissue. Normalizing to the GAPDH signal as a loading control, the overall level of human IDE mRNA expression appeared to vary across tissues and regions of the CNS.

Much of the Variability in IDE mRNA Size Is Due to Alternative Polyadenylation Sites. Since the coding sequence of the known form of IDE is only ∼3.1 kb, we asked to what extent the relatively large size of the predominant ∼5.5 kb transcript could be attributable to the 5′ and 3′ UTRs. Using a 328 bp probe against the genomic sequence 1685−2012 bp downstream of the human IDE stop codon, we detected two transcripts (Figure 1B) that were indistinguishable in size from the two largest transcripts (∼5.5 and ∼9 kb) seen with the catalytic site probe. The relative amounts of the two transcripts within a tissue and the relative amounts of signal among tissues were also indistinguishable from those seen using the catalytic site probe. Of note, there was a strong ∼4.0 kb mRNA exclusively expressed in testis that was not detected by the catalytic site probe.

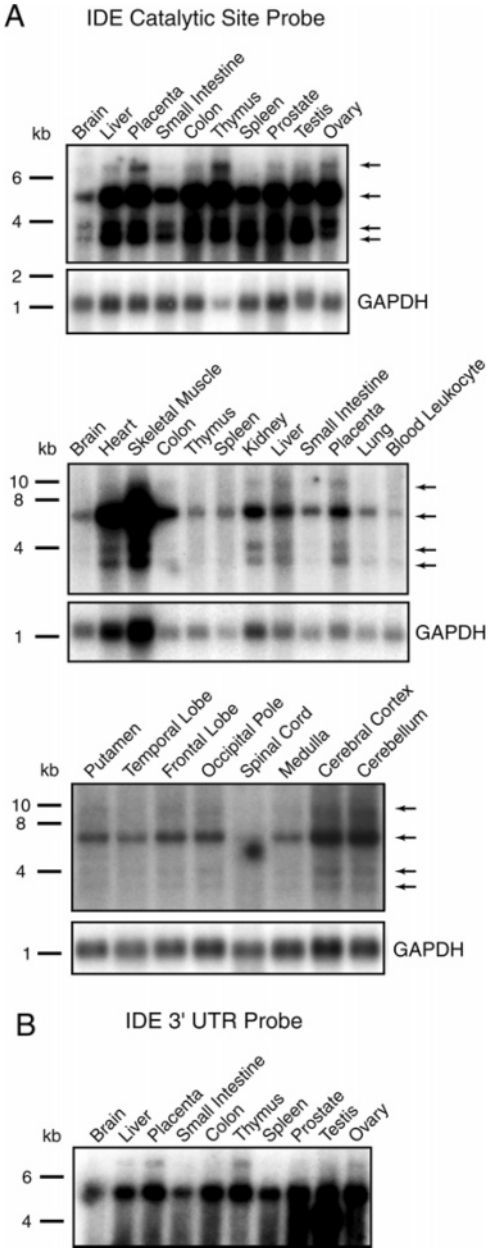

FIGURE 1: Northern blot analysis of human IDE gene expression. (A) A ^{32}P-labeled single-stranded cDNA probe against exons 2 and 3 (containing the catalytic site sequence) was used on Ambion (top) and Clontech (middle and bottom) mRNA blots representing 15 different human tissues and eight different regions of the human CNS. Arrows on the right indicate the position of the four transcripts visualized. Below each IDE catalytic site blot is the same blot striped and reprobed for GAPDH to allow assessment of mRNA loading in each lane. (B) A ^{32}P-labeled cDNA probe against sequence ~2 kb downstream of IDE's stop codon was used on the same Ambion blot pictured in panel A after striping (and thus the GAPDH control in panel A also applies to this blot). Molecular size markers are indicated to the left of each blot.

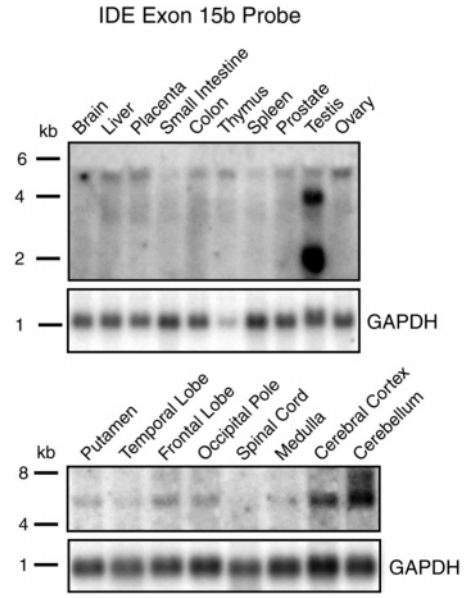

FIGURE 2: Expression of exon 15b of human IDE. A ^{32}P-labeled cDNA probe that exclusively recognizes exon 15b was used to examine the exon's expression in multiple human tissues (Ambion) and eight different human CNS regions (Clontech). Below each exon 15b blot is the same blot striped and reprobed for GAPDH to allow assessment of mRNA loading. Molecular size markers are indicated to the left of each blot.

The known NCBI 25-exon human IDE mRNA (NM_004969) has a 162 bp 3′ UTR and a 57 bp 5′ UTR (Figure 3A, red-shaded regions). 3′ RACE performed with five different sets of nested PCR primers on human brain, liver, testis, and ovary cDNA libraries revealed identical transcript ends 61 and 2033 bp beyond the NCBI mRNA sequence, excluding the RLM-RACE adapter sequences and poly(A) tails, giving 3′ UTRs of 223 and 2195 bp, respectively (Figure 3A). Sequencing of the long 3′-UTR RACE products revealed the canonical polyadenylation signal AAUAAA 13 bp before the start of the poly(A) tail, whereas in the short 3′ UTRs, this hexanucleotide was not present. 5′ RACE experiments performed with nested PCR on the same cDNA libraries showed a variable transcription start site both within and among tissues, ranging from 61 bp shorter than to 22 bp longer than the NCBI sequence (Figure 3A). Interestingly, whereas most of the transcripts included both the first and second potential translational start sites of IDE, the brain did contain a transcript starting at base pair 61, excluding the first ATG at base pairs 58−60.

Thus, assuming a coding region of ~3.1 kb, RACE predicts IDE transcripts of ~3.3 and ~5.3 kb, excluding the poly(A) tail. This is in close agreement with the estimated sizes of two of the major species found by Northern blotting (above). Of note, we did not design RACE primers to identify the ends of the very large ~9 kb transcript, although the above Northern blotting results suggest that its 3′ UTR extends at least 2 kb past the stop codon.

Exon 15b Replaces 15a in a Widely Expressed, Full-Length IDE Splice Variant. We initiated our search for potential splice variants of IDE by assaying for PCR products of unpredicted size from a human liver cDNA library using primer pairs designed to generate overlapping ~500 bp fragments covering the length of the known coding sequence. Each primer pair yielded only one band, and it was of the predicted size for the known 25-exon IDE, suggesting that if splice variants exist, they may not notably change the size of the transcript. We then focused on the two novel exons described in human testis (AK093287) as part of the FLJ human cDNA sequencing project (*34*). In this truncated ~1.9 kb transcript, exons which we designated "11b" (61 bp) and "15b" (145 bp) replace the typical exons "11a" (104 bp) and "15a" (145 bp), respectively, and exons 1−10 are absent. Since the HXXEH catalytic site of IDE is in exon 3, this

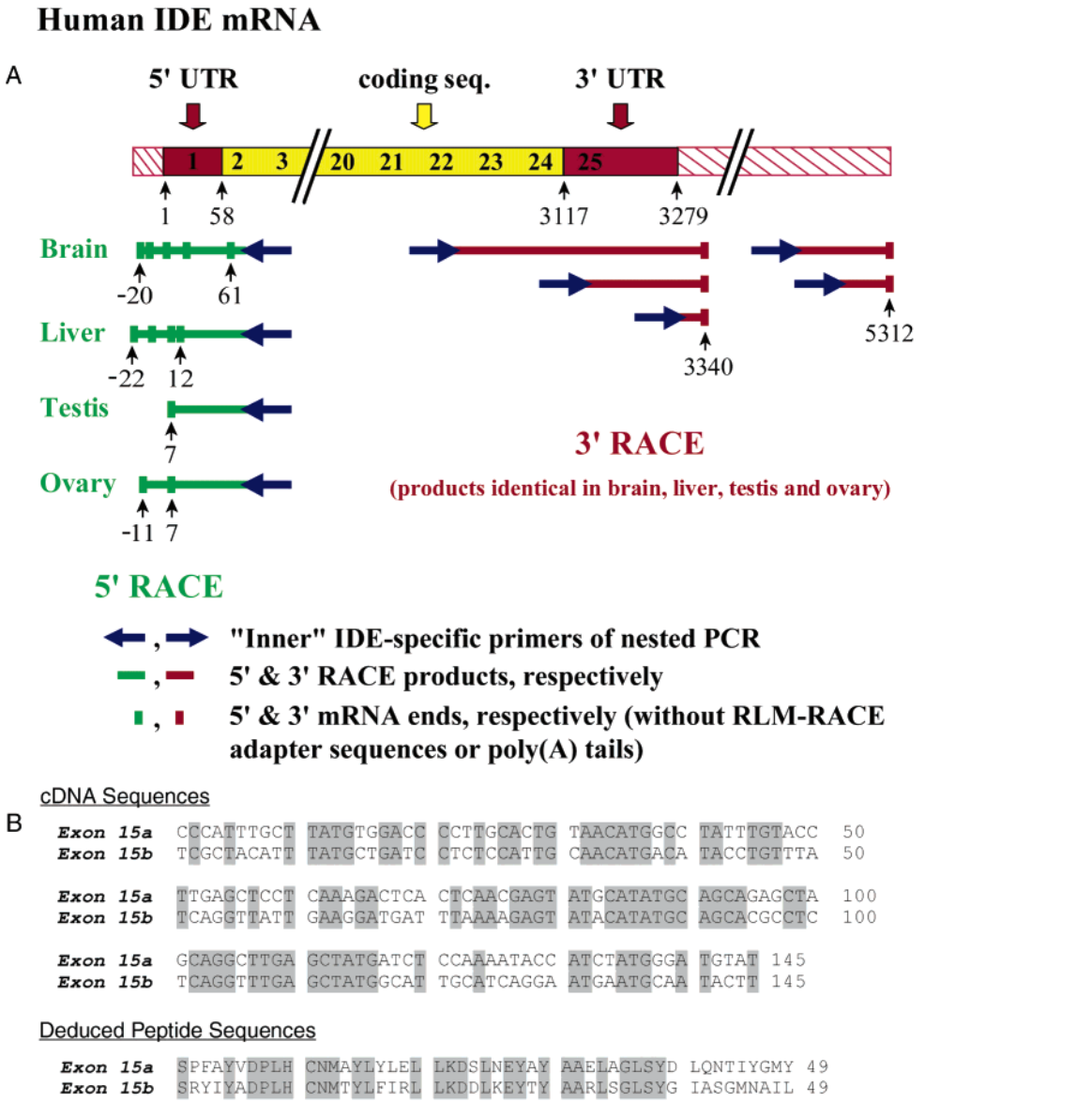

FIGURE 3: Human IDE mRNA. (A) The 25-exon human IDE mRNA is diagrammed with the protein coding sequence in yellow and the UTRs according to NCBI (NM_004969) in red, and extensions of the UTRs that we identified are hatched. The bold numerals superimposed on the mRNA diagram correspond to the exons (not to scale), while the vertical arrows and numbers immediately below it are the transcript's base pair numbers corresponding to the NCBI transcript. Below the transcript diagram are maps of the RACE products [depicted without the RLM-RACE adapter sequences and poly(A) tails], each generated with the inner pair of primers of nested PCR from the human cDNA libraries indicated. Each horizontal marker on a RACE map indicates the end of a separate RACE product that was isolated and sequenced, and the numbering below shows the location of each end in reference to the first base pair of the NCBI transcript. Four to six 5′ RACE experiments (left side) with the same set of nested PCR primers were performed on each cDNA library, usually generating one to two amplicons for sequencing. Each horizontal marker may represent an end identified in only one experiment (as most of the brain mRNA ends) or one seen in every experiment (as the testis mRNA end). 3′ RACE experiments (right side) were carried out with five different sets of nested PCR primers in two duplicate experiments, so each horizontal marker represents the end that was identified in both experiments with each primer set. (B) Sequencing of IDE cDNA cloned from human liver and brain libraries showed that the 145 bp exon 15a can be replaced by the equally sized exon 15b in full-length IDE. In genomic DNA, the beginning of exon 15b is located 487 bp downstream of the end of exon 15a. The two exons' cDNAs and deduced peptide sequences are compared, and an identical sequence is shaded. Of note, the first two base pairs of the codon for the initial serine are in exon 14.

transcript should encode a protein that is not proteolytically active. In an attempt to identify exon 15b in a catalytic site-containing form of IDE and in tissues outside the testis, we probed Northern blots of multiple human tissues and different regions of the human CNS using a 145 bp radiolabeled probe generated against the entire 15b exon, without any adjacent sequence (Figure 2). We validated the specificity of this probe for exon 15b by probing RNA extracted from CHO cells transfected with human 15a-wt-IDE, 15b-wt-IDE, or empty vector (see Experimental Procedures) with both the catalytic site probe and the 15b probe. As expected, the catalytic site probe revealed a single ~3.5 kb transcript in both the 15a-IDE and 15b-IDE RNA lanes, but not the empty vector lane. In contrast, the 15b probe showed a single ~3.5 kb band in the 15b-IDE RNA lane, but no bands in the 15a-IDE or empty vector lanes (not shown). A transcript indistinguishable in size from the major ~5.5 kb transcript seen with the catalytic site probe (Figure 1A) and 3′ UTR probe (Figure 1B) was detected on fresh (i.e., nonstripped) mRNA blots. After prolonged exposure, two additional bands

could be visualized that corresponded to the ~3.5 and ~3.8 kb bands seen earlier with the catalytic site probe. In addition, very strong signals on the exon 15b blot came from two bands found exclusively in testis: a ~2.0 kb transcript and a ~4.0 kb transcript. The latter corresponds to the unique ~4.0 kb band seen in testis with our 3′ UTR probe (Figure 1B). In the cDNA library from testis (but not from brain, liver, or ovary), 5′ RACE using nested PCR within 15b produced an IDE product whose sequence was consistent with the testis 15b-containing transcript from the FLJ sequencing database, but with an additional 17 bp on the 5′ end of the novel exon 11b. Combined with the Northern blot data, the latter result suggests that the difference between the two unique 15b-containing truncated IDE transcripts in the testis is the presence or absence of the ~2 kb 3′ UTR. Full-length 15b-IDE expression levels varied significantly within different regions of the human CNS in a distribution similar to that seen with the catalytic site probe, with highest levels in the cerebral cortex and cerebellum and lowest levels in the spinal cord.

To selectively clone the 15b-containing full-length IDE forms by PCR, two pairs of primers were designed. One primer of each pair was within the 15b sequence, and the other was at either the 5′ or 3′ extreme end of the 25-exon IDE cDNA. Sequencing the entire 15b-containing amplicons from both liver and brain cDNA libraries revealed that exon 15b replaces the identically sized 15a (Figure 3B) in full-length IDE without other splicing changes. When the two exons are compared (Figure 3B), it is evident that the DNA sequences are 57% identical and that the deduced peptide sequences are 53% identical and 69% similar.

The 15b-Containing Protein Isoforms Occur in the Cytosol and Mitochondria, and Targeting Is Determined by Which Translation Start Site Is Used. We examined 15b-IDE for interesting motifs not contained in 15a-IDE using various Internet-based prediction programs [ExPASy Proteomics Server (*39*)]. One program (TMpred, http://www.ch.embnet.org/software/TMPRED_form.html) predicted that exon 15b-IDE contains a transmembrane domain, unlike 15a-IDE, but another program (ALOM subprogram, PSORT II; http://www.psort.org/index.html) predicted that neither isoform would be an integral membrane protein. We recently showed that IDE traffics to mitochondria when translation starts at the first initiation codon, due to the addition of a 41-amino acid N-terminal mitochondrial targeting sequence that is presumably removed after translocation into the organelle (*2*). When the second initiation codon was used, IDE was localized predominantly to the cytosol. For this study, we generated CHO cell lines stably expressing 15b-containing HA-tagged IDE with three possible translational start site configurations (15b-Met1-IDE, 15b-Met42-IDE, and 15b-wt-IDE) and compared the localization and membrane association of IDE in these cells to that in our previously generated CHO cells stably expressing 15a-containing HA-tagged IDE (15a-Met1-IDE, 15a-Met42-IDE, and 15a-wt-IDE) and to a CHO line that stably expresses the empty pcDNA5/FRT vector as a control. We performed subcellular fractionation by differential centrifugation, and the resultant fractions were treated to either maintain organelle integrity (HEPES/HBSS wash) or to rupture organelles (sonication with Na_2CO_3 or urea wash), as described in Experimental Procedures. Each fraction was immunoblotted for levels of HA-tagged IDE as well as for the marker proteins Hsp60 [~85% exists as a soluble mitochondrial matrix protein, with the remainder in various extramitochondrial sites, including the cytosol (*40*)], VDAC (a mitochondrial outer membrane protein), and catalase (a soluble peroxisomal protein). As expected, 15a-Met1-IDE pelleted with mitochondria, 15a-Met42-IDE was in the cytosol, and the majority of 15a-wt-IDE was in the cytosol (Figure 4). Upon prolonged exposure of the immunoblot, 15a-wt-IDE could also be found in the mitochondrial pellet, whereas no 15a-Met42-IDE could be detected in this fraction (data not shown). Washing the mitochondrial pellets with Na_2CO_3 or urea with sonication completely removed the IDE and Hsp60 bands but did not affect the VDAC bands, indicating that the mitochondrial 15a-Met1-IDE is a soluble rather than an integral membrane protein. Like their 15a-IDE counterparts, 15b-Met1-IDE appeared as a non-membrane-associated protein in the mitochondrial fraction, 15b-Met42-IDE was in the cytosol, and 15b-wt-IDE was mostly in the cytosol (Figure 4) with a small amount solubilized from the mitochondria that was seen only upon prolonged exposure (not shown). The peroxisomal marker catalase, found in the HEPES/HBSS-washed 5000*g* and 12000*g* pellets, had a distribution distinct from those of the various IDE isoforms (not shown).

In reference to the predicted transmembrane domain of 15b-IDE, in early experiments, when we simply washed the 15a-wt-IDE and 15b-wt-IDE transiently transfected CHO and COS-7 cells' membrane fraction with Na_2CO_3 (pH 11.3), the 15b isoform consistently appeared to be enriched in the membrane fraction by ~2.5-fold relative to the 15a isoform (data not shown). However, the Na_2CO_3 washes combined with sonication, as described above, eliminated this difference by removing all of the 15b-IDE isoform from the membrane fraction while not affecting the membrane association of the known transmembrane protein VDAC, arguing against 15b-IDE being an integral transmembrane protein. Whether the earlier findings were secondary to Na_2CO_3-resistant nonspecific binding or a true biologic, nonintergral association of the more hydrophobic 15b-IDE with a membrane surface or another membrane-anchored protein is not clear. Of note, cell surface biotinylation followed by immunoprecipitation and immunoblotting for both HA-tagged and endogenous IDE did not reveal IDE on CHO cells either stably or transiently transfected with the various IDE constructs (not shown). As positive controls in these experiments, we were able to detect biotinylated APP on the surface of these same cells and endogenous IDE on the surface of PC12 cells, as previously reported (*35*).

The subcellular localization of the various IDE isoforms in the stably transfected CHO cells was also examined by immunofluorescence confocal microscopy. Both 15a-Met1-IDE and 15b-Met1-IDE colocalized with the mitochondrial marker, cytochrome *c*, whereas 15a-Met42-IDE and 15b-Met42-IDE appeared to be in the cytosol (Figure 5A). 15a-wt-IDE and 15b-wt-IDE mainly occurred in the cytosol, but small amounts of each isoform colocalized with cytochrome *c*. To confirm the localization of the IDE isoforms at the ultrastructural level, we performed immunogold-electron microscopy. Using this method, the IDE signal was fairly weak in the stably transfected cells, so we instead utilized CHO cells transiently overexpressing one of the six IDE

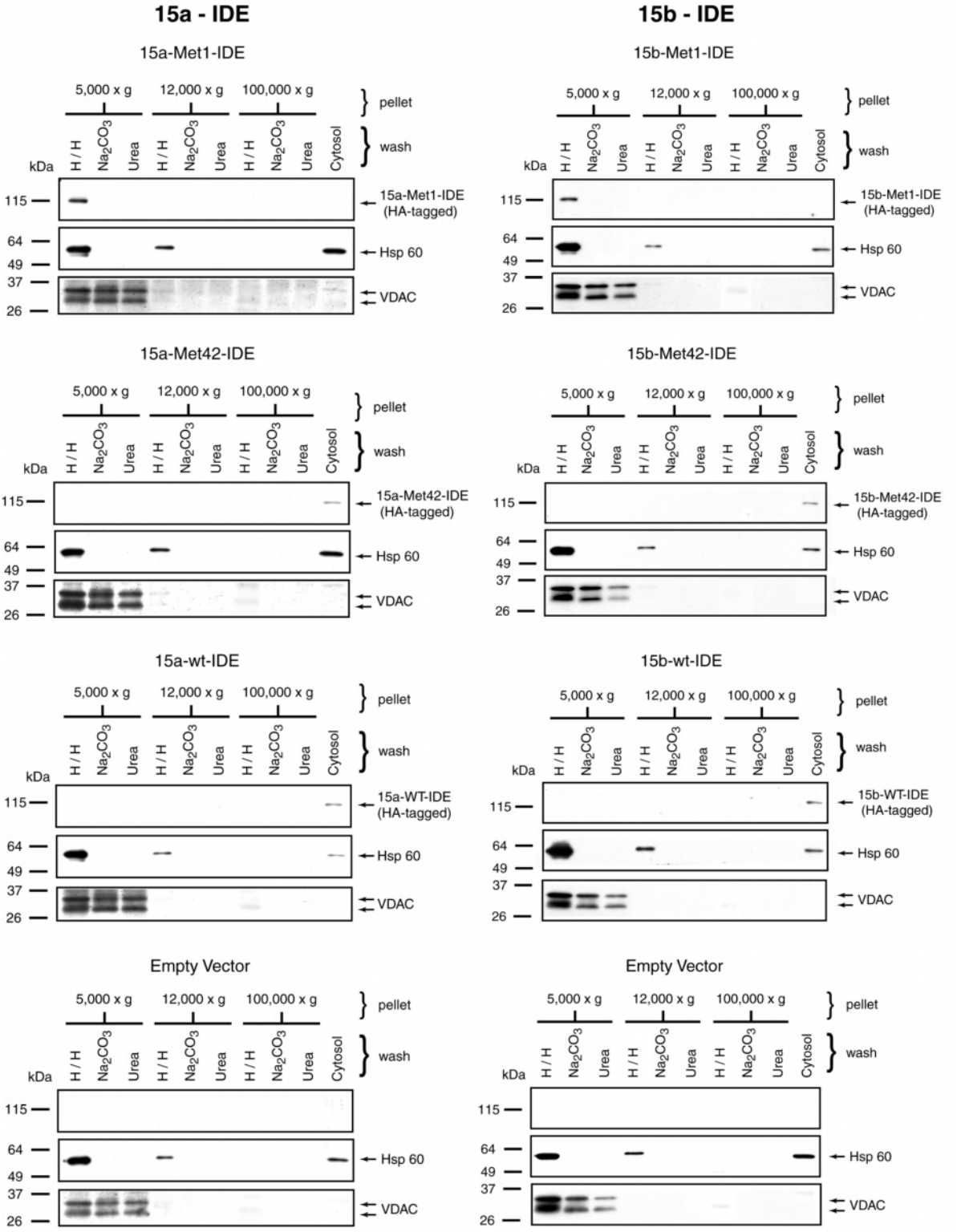

FIGURE 4: Subcellular localization of the different protein isoforms of HA-tagged human IDE by SDS−PAGE/immunoblotting. The postnuclear supernatant from the seven CHO cell lines stably expressing the indicated constructs underwent three subsequent spins at the RCFs shown, generating the three pellet fractions and cytosol. Each pellet fraction was divided into thirds: one washed with HEPES/HBSS ("H/H"), another sonicated and washed with Na_2CO_3 (pH 11.4), and the last sonicated and washed with urea. The amount of material loaded into each lane was derived from an equal number of cells rather than normalizing for protein concentration, allowing direct quantitative comparison of subcellular IDE levels among lanes and across blots. On the left are fractions from CHO lines expressing the 15a-IDE constructs or empty vector that were prepared together, and on the right are fractions from CHO lines expressing the 15b-IDE constructs or empty vector that were prepared together. Each of the eight panels represents one membrane that was cut and immunoblotted with the three indicated antibodies.

constructs or the empty vector control. 15a-Met1-IDE and 15b-Met1-IDE were detected exclusively in mitochondria, whereas 15a-Met42-IDE and 15b-Met42-IDE were in the cytosol (Figure 5B). 15a-wt-IDE and 15b-wt-IDE were detected abundantly in the cytosol with some signal in mitochondria. In contrast to previous work in which the

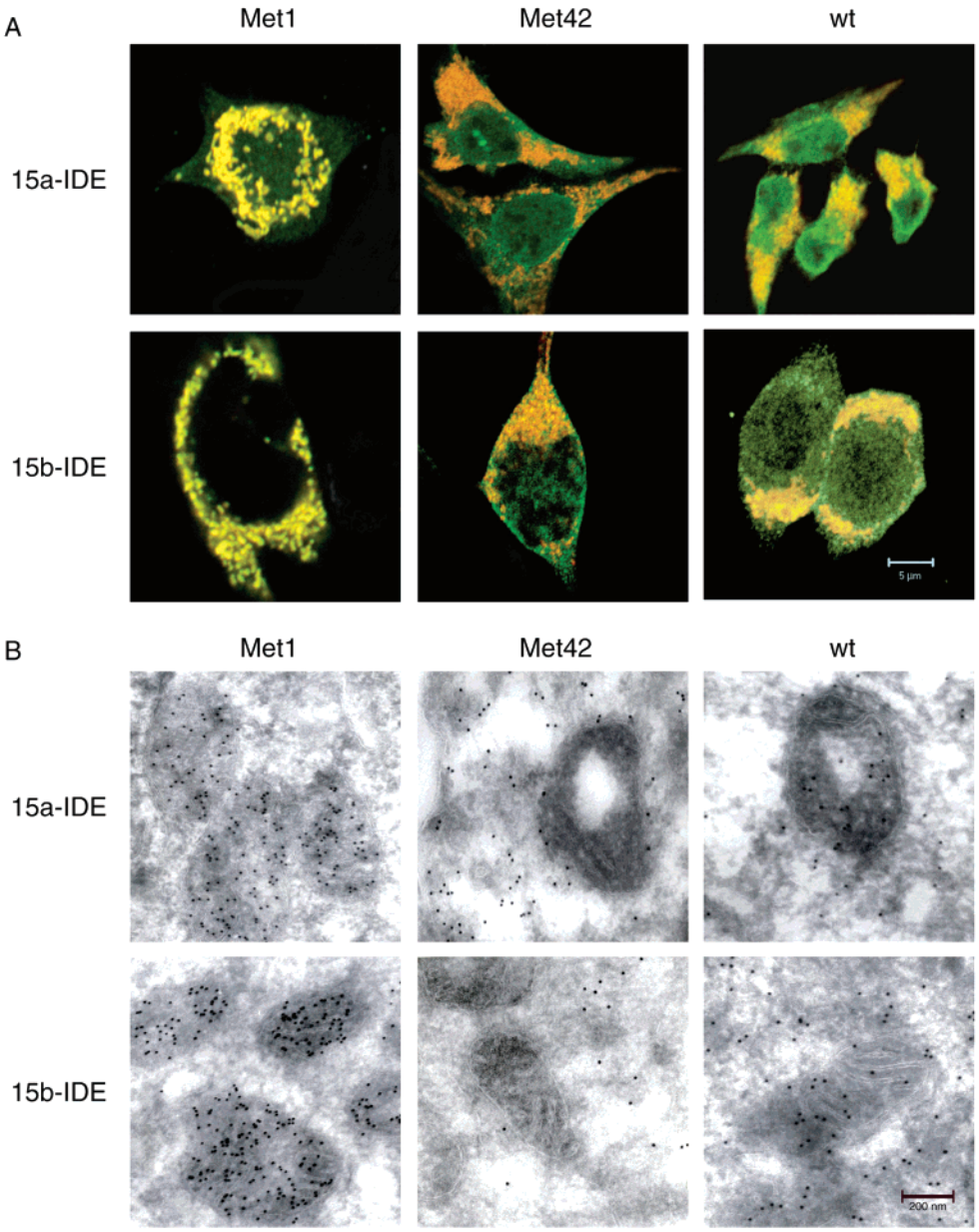

FIGURE 5: Subcellular localization of the different protein isoforms of HA-tagged human IDE by microscopy. (A) Immunofluorescence confocal microscopy with antibodies against the HA tag (green) and cytochrome *c* (red) in CHO cells stably expressing the indicated constructs (15a-IDE constructs in the top row and 15b-IDE constructs in the bottom row). Overlap of the HA tag and cytochrome *c* appears yellow. All images are at the same magnification, and the scale bar at the bottom right represents 5 μm. (B) Immunogold-electron microscopy with antibodies against the HA tag on CHO cells transiently expressing the indicated constructs (15a-IDE constructs in the top row and 15b-IDE constructs in the bottom row). Images are at 25000× magnification, and the scale bar at the bottom right represents 200 nm.

location of transfected IDE was examined in Ltk$^-$ mouse fibroblasts by immunogold-electron microscopy (*41*), we were unable to find colocalization of IDE with catalase in CHO cells (data not shown).

Human 15a- and 15b-IDE Can Exist as Homodimers or Heterodimers. Rat IDE has been shown to exist predominately as a dimer and possibly as a tetramer (*42*). To examine the oligomeric nature of human 15a- and 15b-IDE, we first generated recombinant forms of 15a-Met42-IDE and 15b-Met42-IDE, and then analyzed each of them by Blue Native-PAGE, which separates intact protein complexes approximately by molecular weight under nonreducing and nondenaturing conditions. Each of the recombinant IDE isoforms appeared exclusively as a complex of ~220 kDa by Coomassie Blue staining, consistent with its existence as a homodimer (Figure 6A). When lysates from COS-7 cells transiently transfected with the HA-tagged 15a- or 15b-wt-IDE construct were analyzed by Blue Native-PAGE and immunoblotting with an anti-HA antibody, a single band of ~220 kDa was seen, indicating that human IDE within cells also primarily exists as a dimer (not shown). To confirm the dimeric nature of human IDE within cells and to determine whether IDE can exist in part as a heterodimer of the 15a- and 15b-IDE isoforms, we coexpressed in CHO cells a C-terminally V5-tagged 15a-wt-IDE construct with either the HA-tagged 15a-wt-IDE or HA-tagged 15b-wt-IDE construct. Immunoprecipitation with an anti-HA antibody matrix followed by SDS−PAGE and immunoblotting with an anti-V5 antibody revealed coprecipitation of the V5-tagged 15a-IDE with both the HA-tagged 15a- and 15b-IDEs

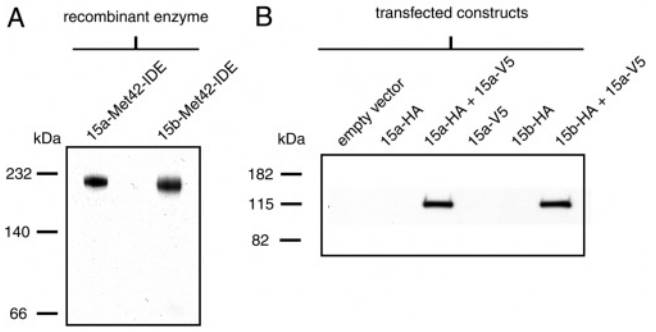

FIGURE 6: Dimerization of 15a- and 15b-IDE. (A) Blue-native gel electrophoresis and Coomassie Blue staining of recombinant human 15a-Met42-IDE and 15b-Met42-IDE. (B) Co-immunoprecipitation/immunoblotting of lysates from CHO cells transiently transfected with the empty vector, the V5-tagged 15a-wt-IDE (15a-V5) construct, and/or the HA-tagged 15a- or 15b-wt-IDE (15a-/15b-HA) construct. The material immunoprecipitated with the anti-HA matrix was subjected to SDS−PAGE and immunoblotted with the antibody against the V5 tag.

(Figure 6B). Identically treated lysates from cells transfected with any one of the constructs alone yielded no bands, while immunoblotting of straight lysates with antibodies against the HA and V5 tags confirmed successful expression of each construct (not shown). Thus, within cells, the canonical human 15a-IDE can apparently exist as heterodimers with 15b-IDE and as homodimers.

15b-IDE Has Kinetic Properties Significantly Different from Those of 15a-IDE for both Insulin and Aβ Substrates. Although not occurring at a position necessarily adjacent to the enzyme's catalytic site in exon 3, the alternative splicing of exon 15 could nonetheless have important consequences for the proteolytic function of IDE. To test this hypothesis, we compared the kinetics of hydrolysis of human insulin and human Aβ_{40} by recombinant human 15a- and 15b-IDE, using well-established iodinated peptide degradation assays (*5*). The resultant data are represented by double-reciprocal plots (Figure 7), and for greater accuracy, the kinetic parameters in Tables 1 and 2 were determined by hyperbolic regression analysis, as previously described (*37*). Recombinant 15a-IDE yielded apparent K_m values of 66 nM and 1.2 μM for insulin (Figure 7A) and Aβ (Figure 7B), respectively, which is consistent with values obtained using other sources of recombinant or purified human IDE (*37*, *43*). In contrast, the 15b isoform yielded significantly higher K_m values for

Table 1: Human [^{125}I]Insulin as a Substrate of Recombinant Human IDE[a]

parameter	15a-IDE	15b-IDE	*P* value[b]
K_m (nM)	65.7 ± 3.4	222 ± 7	<0.05
k_{cat} (min^{-1})	1.52 ± 0.02	1.01 ± 0.03	<0.05
k_{cat}/K_m (M^{-1} min^{-1})	23.14 × 10^6	4.55 × 10^6	<0.05

[a] Values are the mean ± the standard deviation of two to three independent experiments. [b] *P* values are for differences between 15a- and 15b-IDE as determined by a Student's *t*-test.

Table 2: Human [^{125}I]Aβ_{40} as a Substrate of Recombinant Human IDE[a]

parameter	15a-IDE	15b-IDE	*P* value[b]
K_m (nM)	1230 ± 96	2520 ± 40	<0.05
k_{cat} (min^{-1})	52.5 ± 0.2	11.0 ± 0.3	<0.005
k_{cat}/K_m (M^{-1} min^{-1})	42.72 × 10^6	4.37 × 10^6	<0.05

[a] Values are the mean ± the standard deviation of two to three independent experiments. [b] *P* values are for differences between 15a- and 15b-IDE as determined by a Student's *t*-test.

both insulin (Figure 7A) and Aβ (Figure 7B), namely, 222 nM and 2.5 μM, respectively. The k_{cat} values for insulin and Aβ proteolysis were also significantly decreased for 15b-IDE relative to the 15a isoform (Tables 1 and 2). Thus, the catalytic efficiency (k_{cat}/K_m) of 15b-IDE for insulin (Table 1) and Aβ (Table 2) is only ~20 and ~10%, respectively, of those of 15a-IDE.

Intact Cells Overexpressing 15b-IDE Accumulate Significantly More Aβ in Their Media than Those Overexpressing 15a-IDE. To determine whether the above kinetic differences between 15a- and 15b-IDE translate into differences in the catabolism of endogenously produced Aβ in living cells, we transiently transfected equal amounts of either 15a-wt-IDE or 15b-wt-IDE cDNAs into a CHO cell line stably expressing human APP and measured the levels of Aβ in the conditioned media with an ELISA. The two IDE isoforms were expressed at equal levels, as assessed by immunoblotting (Figure 8B). Compared to the conditioned media from cells transfected with the canonical 15a-IDE, the media from 15b-IDE-transfected cells had a 2.2-fold elevation in the levels of Aβ X-40 ($P < 0.005$, two-tailed Student's *t*-test) and a 2.0-fold increase in the levels of Aβ X-42 ($P < 0.01$) (Figure 8A). The media from cells transfected with the empty vector had 4.0- and 3.9-fold more Aβ X-40 and Aβ X-42 than did the

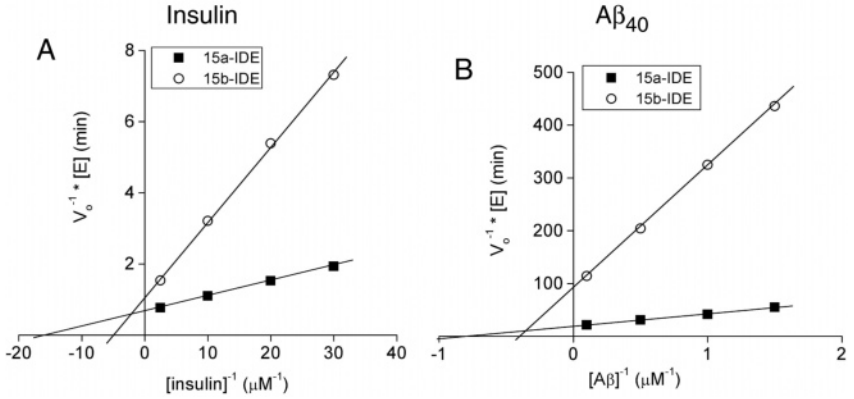

FIGURE 7: Kinetic analysis of insulin and Aβ_{40} degradation by recombinant 15a- and 15b-IDE. Double-reciprocal plots for the degradation of [^{125}I]insulin (A) or [^{125}I]Aβ_{40} (B) by recombinant human 15a- or 15b-IDE. Initial velocities (V_0) were determined by incubation of the proteases with various concentrations of substrate using trichloroacetic acid precipitation assays. Data represent the average of two to three experiments per condition and have been normalized to reflect the different concentrations of recombinant enzymes (E) used in the assays.

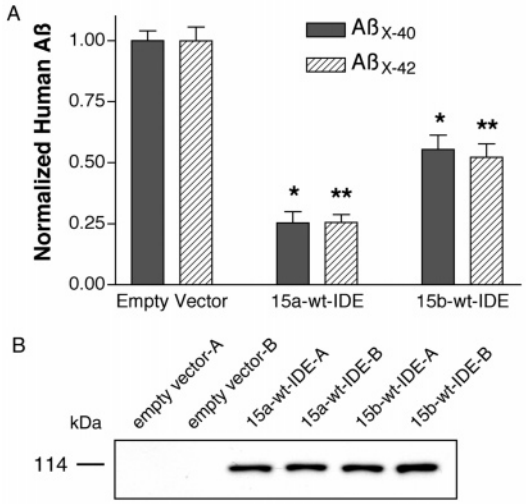

FIGURE 8: Human Aβ levels in the conditioned media of cells overexpressing 15a- or 15b-IDE. (A) CHO cells stably expressing human APP_{751} with the V717F AD-causing missense mutation were transiently transfected with the empty vector, 15a-wt-IDE, or 15b-wt-IDE. Media were conditioned on the cells for 18 h, and their Aβ levels were determined with an ELISA. Data represent means $\pm$ the standard error of the mean of 8−12 determinations from four to six transfection experiments measured in duplicate in three independent ELISA runs after normalizing to the empty vector Aβ values in each run to allow combination of the data sets ($P < 0.0001$ for differences in Aβ X-40 and Aβ X-42 levels between empty vector and 15a-IDE or 15b-IDE). One asterisk means $P < 0.005$ for the difference between 15a- and 15b-IDE; two asterisks mean $P < 0.01$ for the difference between 15a- and 15b-IDE. (B) A representative immunoblot (anti-HA) from a transfection experiment confirms equal expression of 15a- and 15b-wt-IDE. Each construct was transfected into duplicate dishes, A and B.

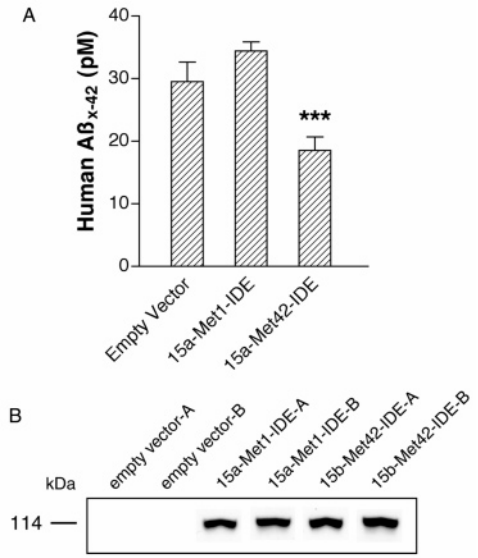

FIGURE 9: Human Aβ levels in the conditioned media of cells overexpressing Met1- or Met42-IDE. (A) CHO cells stably expressing human APP were transiently transfected with the empty vector, 15a-Met1-IDE, or 15a-Met42-IDE. Media were conditioned for 18 h, and their Aβ levels were determined with an ELISA. Data represent means $\pm$ the standard error of the mean of four determinations from two transfection experiments measured in duplicate with an ELISA. Three asterisks mean $P < 0.05$ for the empty vector vs 15a-Met42-IDE, $P < 0.001$ for 15a-Met1-IDE vs 15a-Met42-IDE, and P is not significant for the empty vector vs 15a-Met1-IDE. (B) A representative anti-HA immunoblot from a transfection experiment confirms equal expression of the IDE isoforms. Each construct was transfected into duplicate dishes, A and B.

15a-IDE conditioned media, respectively, and 1.8- and 1.9-fold more Aβ X-40 and Aβ X-42 than the 15b-IDE conditioned media, respectively ($P < 0.0001$ for each comparison).

Only IDE Isoforms Utilizing the Second Translational Start Site Regulate the Levels of Secreted Aβ. It has recently been suggested that intracellular $A\beta_{42}$ exists predominately in the mitochondria, where it causes oxidative stress (*44*). To establish which pool of IDE (mitochondrial or cytosolic) is capable of regulating the levels of secreted Aβ, we compared the levels of Aβ X-42 in the conditioned media of the APP-overexpressing CHO lines transiently transfected with 15a-Met1-IDE and 15a-Met42-IDE. Equal expression of each isoform was again confirmed by immunoblotting (Figure 9B). Aβ X-42 levels in media from 15a-Met1-IDE-expressing cells were not significantly different than those from cells transfected with the empty vector, whereas 15a-Met42-IDE-transfected cells had significantly lower levels of Aβ ($P < 0.05$) (Figure 9A), like the wt-IDE transfections described above. Measurement of Aβ X-40 levels gave similar results (not shown). Thus, only IDE isoforms lacking the mitochondrial targeting sequence appear to be relevant in regulating the levels of secreted Aβ in intact cells.

DISCUSSION

In this study, we have (1) characterized the transcripts of human IDE, (2) found that alternative poly(A) sites are used, (3) discovered the first full-length and first widely expressed IDE splice variant, (4) showed that the corresponding protein isoform, like the known one, can occur in the cytosol and mitochondria and that trafficking is determined by which translational start site is used, (5) demonstrated that the two human IDE variants can exist as either homodimers or heterodimers, (6) established that the novel isoform has a significantly higher K_m and lower catalytic efficiency for both insulin and Aβ than the known form and that this difference is biologically relevant in intact cells, and (7) showed that only IDE isoforms utilizing the second translational start site regulate the levels of secreted Aβ.

Characterization of IDE Transcripts. Our results show that there are at least six different-sized human IDE transcripts: four with a wide tissue distribution (~3.5, ~3.8, ~5.5, and ~9 kb) and two exclusive to testis (~2.0 and ~4.0 kb). All four of the multitissue transcripts contain the catalytic site sequence, whereas neither of the testis-specific transcripts does. The widely distributed ~3.5 kb mRNA band is consistent with the 25-exon IDE mRNA in the NCBI database with the addition of both the 61 bp of 3′ UTR that we identified by RACE and the poly(A) tail. The ~5.5 kb transcript was the major species in every tissue except testis, and it appeared to be identical to the ~3.5 kb mRNA except for an additional ~2 kb of 3′ UTR. The significance of IDE's unusually long and variably sized 3′ UTRs requires further investigation, but it is interesting to note the accumulating evidence demonstrating that 3′ UTRs play an important role in regulation of mRNA stability, control of mRNA subcellular localization, and efficiency of mRNA translation (*45*). The faint ~9 kb species also contained 3′ UTRs of at least 2 kb, and we hypothesize that the large size of these transcripts is due to their 3′ UTRs. Although we did not

design Northern probes or RACE primers to explore the 3′ UTR of this minor mRNA, inspection of the genomic sequence revealed a polyadenylation signal ~3.7 kb downstream of the 3′ end of the ~5.5 kb transcript.

In contrast to the several human IDE transcripts we identified, only two widely distributed mRNAs have been described in rat (~3.5 and ~6 kb) (*31*, *32*) and *Drosophila* (~3.6 and ~6.3 kb) (*30*). Although the human ~3.8 and ~9 kb mRNAs do not appear to have rat or *Drosophila* orthologues, all four of the multitissue human transcripts were detected by at least two different nonoverlapping probes, suggesting that our Northern bands all represent bona fide IDE mRNAs. Like the ~5.5 kb human transcript, the ~6 kb rat mRNA was the major species, but in *Drosophila*, the smaller ~3.6 kb band predominated.

Rats have also been shown to have two unique transcripts in the testis, but only one of these appears to be homologous to the human testis mRNAs we describe. Both rats and humans have a ~4 kb testis transcript, and our work suggests that in humans this consists of the known ~1.9 kb 5′-truncated IDE mRNA with the addition of an ~2 kb 3′ UTR. The probes used to examine rat IDE transcripts (*31*, *32*) were designed for sequences that would be present in a similarly 5′-truncated rat mRNA, so the ~4 kb rat testis transcript may represent an orthologue to the equally sized human form. We did not detect a testis-specific transcript similar to the ~6.5 kb rat testis mRNA, but we did detect a very strong band in testis ~2.0 kb length using the 15b probe, probably representing the known 5′-truncated mRNA without the long 3′ UTR. The fact that one of these testis transcripts lacking the catalytic site sequence may be evolutionarily conserved in rat raises the question of whether it has a nonproteolytic biological function. In this regard, there have been several functions attributed to IDE that do not directly involve proteolysis, including regulation of the proteasome (*46*) and interaction with steroid receptors (*47*), and perhaps this form of the protein has such a role.

Our 5′ RACE experiments show that the transcription start site is "slippery", suggestive of a CpG island promoter. Examination of the *IDE* gene for CpG-rich regions using the NCBI Genome website algorithm with the "strict" criteria of Takai and Jones (*48*) revealed only one such region in the entire ~120 kb gene. This ~1.8 kb CpG island contains exon 1 and includes ~800 bp of genomic sequence upstream of the transcriptional start site of the mRNA with the longest 5′ UTR. Also compatible with a CpG island-type promoter for *IDE* are the transcripts' wide tissue distribution, and the inability to identify any other canonical promoter sequences associated with the gene. In the brain, the 5′ mRNA ends varied by up to 80 bp, with the shortest 5′ end lacking the first coding ATG, thus forcing translation to begin at the second ATG and presumably resulting in the localization of the protease to the cytosol rather than the mitochondria. This result raises the intriguing possibility that cells utilize alternative transcription start sites to regulate the trafficking of IDE, but further investigation is necessary to confirm this.

Identification, localization, and Activity of 15b-IDE. We found that the 145 bp exon 15b can replace the equally sized exon 15a in full-length IDE, and that this species is widely expressed at low levels in multiple tissues, including in multiple brain regions. The fact that this newly identified spliceoform does not result in a perceptible change in the molecular weight of the protease is compatible with much previous data showing that by SDS−PAGE and immunoblotting (using several different anti-IDE antibodies) there is a single endogenous IDE protein band.

Subcellular fractionation, cell surface biotinylation, immunofluorescence confocal microscopy, and immunogold-electron microscopy all indicated that both 15a- and 15b-wt-IDE were predominately in the cytosol, with smaller amounts in the soluble phase of mitochondria and none on the cell surface. This is only in partial agreement with earlier reports (*35*) in which similar methods were used on various cell types to localize IDE to the cytosol, and variably to the cell surface, endosomes, or predominantly peroxisomes (*1*, *41*, *49*). The results suggest that the subcellular distribution of IDE may vary by cell type. In our CHO cell model, only the cytosolic IDE isoforms regulated the levels of secreted Aβ. This finding is consistent with a recent report suggesting that IDE degrades Aβ via endoplasmic reticulum-associated degradation, in which the endoplasmic reticulum-localized Aβ is translocated into the cytosol where it is degraded by IDE (*50*). Presumably, at least a portion of the Aβ that escapes the endoplasmic reticulum-associated degradation represents the secreted Aβ measured in our experiments.

Alternative splicing of exon 15 has a significant impact on the enzyme's ability to degrade insulin and Aβ, even though the two isoforms are fairly similar in terms of primary sequence. Interestingly, the K_m for insulin is affected relatively more than for Aβ when exon 15b replaces 15a, whereas the k_{cat} is altered more for Aβ than insulin. Ultimately, both the decrease in k_{cat} and the increase in K_m cause the 15b isoform of IDE to be much less efficient at degrading both insulin and Aβ than the 15a variant (~20 and ~10% as efficient, respectively). These data argue that exon 15a serves an important role in sustaining the normal proteolytic activity of IDE, perhaps as a substrate-binding site or in maintaining the protease's tertiary structure. It is noteworthy that the turnover number (k_{cat}) for insulin by both 15a- and 15b-IDE is significantly lower than that for Aβ. This means that if IDE were saturated with a single substrate, using k_{cat} as a measure, the 15a isoform would cleave Aβ ~35 times more rapidly than insulin, while 15b-IDE would degrade Aβ ~11 times faster than insulin.

The kinetic parameters were determined on recombinant 15a- and 15b-IDE, which we showed exist entirely as homodimers (Figure 6A). We demonstrated that within cells, human IDE can exist as heterodimers of the 15a and 15b isoforms, suggesting that this third species of IDE dimer could have unique kinetic properties distinct from those of the two types of homodimers we examined, possibly with kinetic constant values between those of the two homodimers. Whether cells regulate the alternative splicing of exons 15a and 15b to control the overall proteolytic activity of the pool of IDE dimers is a question for further investigation.

Potential Medical Relevance of These Findings. In addition to expanding our understanding of the normal biology of IDE, our findings may also have direct medical relevance. Despite an increasing number of human genetic studies supporting IDE as a susceptibility gene for AD and DM2, none of the single-nucleotide polymorphisms identified to date in the coding regions appear to be pathogenic mutations. In this study, we describe a novel splice variant that exists in tissues relevant for AD (brain) and DM2 (liver) and

characterize two noncoding regions that could have regulatory functions, the 5′ and 3′ UTRs. Anomalies in the 3′ UTR have been shown to play a role in several human diseases, including myotonic dystrophy, α-thalassemia, and certain neoplastic disorders (*45*). By identifying both a previously undescribed IDE splice variant in disease-relevant tissues that markedly reduces proteolytic efficiency and the unusually long 3′ UTRs of some IDE transcripts, our work points to new regions of the IDE gene in which to search for disease-causing genetic alterations. Whether mutations in IDE cause some cases of AD or DM2, a better understanding of IDE biology is warranted for at least two reasons. First, IDE could still have a nongenetic role in the pathophysiology of these common diseases, and second, IDE is a rational target for therapeutic manipulation. Besides the in vivo functional data from gene-deleted animals, several other findings suggest that IDE may play a pathophysiological role, independent of any genetic alterations: (1) IDE levels are reduced in the brains of diabetic APP transgenic mice, which have increased cerebral Aβ levels compared to nondiabetic APP transgenic controls (*51*); (2) IDE levels are decreased in the hippocampi of AD patients who have an apolipoprotein E ϵ4 allele (*52*); and (3) IDE activity may be diminished in AD brain fractions relative to controls (*53*). We have recently shown that chronic overexpression of human IDE in the neurons of an APP transgenic mouse model of AD results in significantly lower levels of cerebral Aβ, fewer amyloid plaques, and prevention of premature death (*2*). These in vivo findings advocate attempting to increase the activity of IDE as a treatment strategy in AD, whether by directly increasing the catalytic efficiency, increasing the protease's expression, or blocking a natural IDE inhibitor.

ACKNOWLEDGMENT

We thank Maria Ericsson for the immunogold-electron microscopy, Jacqueline Sears and Weiming Xia for several of the ELISAs, Dominic Walsh for providing the CHO line stably transfected with the pFRT/lacZeo vector of the Flp-In system, and Jay Chung, Matthew LaVoie, Beth Ostaszewski, Anna Krichevsky, and Sally Agersborg for technical advice.

REFERENCES

1. Duckworth, W. C., Bennett, R. G., and Hamel, F. G. (1998) Insulin degradation: Progress and potential, *Endocr. Rev. 19*, 608−624.
2. Leissring, M. A., Farris, W., Wu, X., Christodoulou, D. C., Haigis, M. C., Guarente, L., and Selkoe, D. J. (2004) Alternative translation initiation generates a novel isoform of insulin-degrading enzyme targeted to mitochondria, *Biochem. J. 383*, 439−446.
3. Edbauer, D., Willem, M., Lammich, S., Steiner, H., and Haass, C. (2002) Insulin-degrading enzyme rapidly removes the β-amyloid precursor protein intracellular domain (AICD), *J. Biol. Chem. 277*, 13389−13393.
4. Bennett, R. G., Duckworth, W. C., and Hamel, F. G. (2000) Degradation of amylin by insulin-degrading enzyme, *J. Biol. Chem. 275*, 36621−36625.
5. Farris, W., Mansourian, S., Chang, Y., Lindsley, L., Eckman, E. A., Frosch, M. P., Eckman, C. B., Tanzi, R. E., Selkoe, D. J., and Guenette, S. (2003) Insulin-degrading enzyme regulates the levels of insulin, amyloid β-protein, and the β-amyloid precursor protein intracellular domain in vivo, *Proc. Natl. Acad. Sci. U.S.A. 100*, 4162−4167.
6. Miller, B. C., Eckman, E. A., Sambamurti, K., Dobbs, N., Chow, K. M., Eckman, C. B., Hersh, L. B., and Thiele, D. L. (2003) Amyloid-β peptide levels in brain are inversely correlated with insulysin activity levels in vivo, *Proc. Natl. Acad. Sci. U.S.A. 100*, 6221−6226.
7. Farris, W., Mansourian, S., Leissring, M. A., Eckman, E. A., Bertram, L., Eckman, C. B., Tanzi, R. E., and Selkoe, D. J. (2004) Partial loss-of-function mutations in insulin-degrading enzyme that induce diabetes also impair degradation of amyloid β-protein, *Am. J. Pathol. 164*, 1425−1434.
8. Bertram, L., Blacker, D., Mullin, K., Keeney, D., Jones, J., Basu, S., Yhu, S., McInnis, M. G., Go, R. C., Vekrellis, K., Selkoe, D. J., Saunders, A. J., and Tanzi, R. E. (2000) Evidence for genetic linkage of Alzheimer's disease to chromosome 10q, *Science 290*, 2302−2303.
9. Ghosh, S., Watanabe, R. M., Valle, T. T., Hauser, E. R., Magnuson, V. L., Langefeld, C. D., Ally, D. S., Mohlke, K. L., Silander, K., Kohtamaki, K., Chines, P., Balow, J., Jr., Birznieks, G., Chang, J., Eldridge, W., Erdos, M. R., Karanjawala, Z. E., Knapp, J. I., Kudelko, K., Martin, C., Morales-Mena, A., Musick, A., Musick, T., Pfahl, C., Porter, R., and Rayman, J. B. (2000) The Finland-United States investigation of non-insulin-dependent diabetes mellitus genetics (FUSION) study. I. An autosomal genome scan for genes that predispose to type 2 diabetes, *Am. J. Hum. Genet. 67*, 1174−1185.
10. Wiltshire, S., Hattersley, A. T., Hitman, G. A., Walker, M., Levy, J. C., Sampson, M., O'Rahilly, S., Frayling, T. M., Bell, J. I., Lathrop, G. M., Bennett, A., Dhillon, R., Fletcher, C., Groves, C. J., Jones, E., Prestwich, P., Simecek, N., Rao, P. V., Wishart, M., Bottazzo, G. F., Foxon, R., Howell, S., Smedley, D., Cardon, L. R., Menzel, S., and McCarthy, M. I. (2001) A genomewide scan for loci predisposing to type 2 diabetes in a U.K. population (the Diabetes UK Warren 2 Repository): Analysis of 573 pedigrees provides independent replication of a susceptibility locus on chromosome 1q, *Am. J. Hum. Genet. 69*, 553−569.
11. Meigs, J. B., Panhuysen, C. I., Myers, R. H., Wilson, P. W., and Cupples, L. A. (2002) A genome-wide scan for loci linked to plasma levels of glucose and HbA(1c) in a community-based sample of Caucasian pedigrees: The Framingham Offspring Study, *Diabetes 51*, 833−840.
12. Ait-Ghezala, G., Abdullah, L., Crescentini, R., Crawford, F., Town, T., Singh, S., Richards, D., Duara, R., and Mullan, M. (2002) Confirmation of association between D10S583 and Alzheimer's disease in a case-control sample, *Neurosci. Lett. 325*, 87−90.
13. Edland, S. D., Wavrant-De Vriese, F., Compton, D., Smith, G. E., Ivnik, R., Boeve, B. F., Tangalos, E. G., and Petersen, R. C. (2003) Insulin degrading enzyme (IDE) genetic variants and risk of Alzheimer's disease: Evidence of effect modification by apolipoprotein E (APOE), *Neurosci. Lett. 345*, 21−24.
14. Prince, J. A., Feuk, L., Gu, H. F., Johansson, B., Gatz, M., Blennow, K., and Brookes, A. J. (2003) Genetic variation in a haplotype block spanning IDE influences Alzheimer disease, *Hum. Mutat. 22*, 363−371.
15. Bian, L., Yang, J. D., Guo, T. W., Sun, Y., Duan, S. W., Chen, W. Y., Pan, Y. X., Feng, G. Y., and He, L. (2004) Insulin-degrading enzyme and Alzheimer disease: A genetic association study in the Han Chinese, *Neurology 63*, 241−245.
16. Ertekin-Taner, N., Allen, M., Fadale, D., Scanlin, L., Younkin, L., Petersen, R. C., Graff-Radford, N., and Younkin, S. G. (2004) Genetic variants in a haplotype block spanning IDE are significantly associated with plasma Aβ42 levels and risk for Alzheimer disease, *Hum. Mutat. 23*, 334−342.
17. Karamohamed, S., Demissie, S., Volcjak, J., Liu, C., Heard-Costa, N., Liu, J., Shoemaker, C. M., Panhuysen, C. I., Meigs, J. B., Wilson, P., Atwood, L. D., Cupples, L. A., and Herbert, A. (2003) Polymorphisms in the Insulin-Degrading Enzyme Gene Are Associated With Type 2 Diabetes in Men From the NHLBI Framingham Heart Study, *Diabetes 52*, 1562−1567.
18. Gu, H. F., Efendic, S., Nordman, S., Ostenson, C. G., Brismar, K., Brookes, A. J., and Prince, J. A. (2004) Quantitative trait loci near the insulin-degrading enzyme (IDE) gene contribute to variation in plasma insulin levels, *Diabetes 53*, 2137−2142.
19. Abraham, R., Myers, A., Wavrant-DeVrieze, F., Hamshere, M. L., Thomas, H. V., Marshall, H., Compton, D., Spurlock, G., Turic, D., Hoogendoorn, B., Kwon, J. M., Petersen, R. C., Tangalos, E., Norton, J., Morris, J. C., Bullock, R., Liolitsa, D., Lovestone, S., Hardy, J., Goate, A., O'Donovan, M., Williams, J., Owen, M. J., and Jones, L. (2001) Substantial linkage disequilibrium across the insulin-degrading enzyme locus but no association with late-onset Alzheimer's disease, *Hum. Genet. 109*, 646−652.
20. Boussaha, M., Hannequin, D., Verpillat, P., Brice, A., Frebourg, T., and Campion, D. (2002) Polymorphisms of insulin degrading enzyme gene are not associated with Alzheimer's disease, *Neurosci. Lett. 329*, 121−123.

21. Sakai, A., Ujike, H., Nakata, K., Takehisa, Y., Imamura, T., Uchida, N., Kanzaki, A., Yamamoto, M., Fujisawa, Y., Okumura, K., and Kuroda, S. (2004) No association between the insulin degrading enzyme gene and Alzheimer's disease in a Japanese population, *Am. J. Med. Genet. 125B*, 87−91.
22. Groves, C. J., Wiltshire, S., Smedley, D., Owen, K. R., Frayling, T. M., Walker, M., Hitman, G. A., Levy, J. C., O'Rahilly, S., Menzel, S., Hattersley, A. T., and McCarthy, M. I. (2003) Association and haplotype analysis of the insulin-degrading enzyme (IDE) gene, a strong positional and biological candidate for type 2 diabetes susceptibility, *Diabetes 52*, 1300−1305.
23. Leibson, C. L., Rocca, W. A., Hanson, V. A., Cha, R., Kokmen, E., O'Brien, P. C., and Palumbo, P. J. (1997) Risk of dementia among persons with diabetes mellitus: A population-based cohort study, *Am. J. Epidemiol. 145*, 301−308.
24. Ott, A., Stolk, R. P., van Harskamp, F., Pols, H. A., Hofman, A., and Breteler, M. M. (1999) Diabetes mellitus and the risk of dementia: The Rotterdam Study, *Neurology 53*, 1937−1942.
25. Luchsinger, J. A., Tang, M. X., Stern, Y., Shea, S., and Mayeux, R. (2001) Diabetes mellitus and risk of Alzheimer's disease and dementia with stroke in a multiethnic cohort, *Am. J. Epidemiol. 154*, 635−641.
26. Peila, R., Rodriguez, B. L., and Launer, L. J. (2002) Type 2 diabetes, APOE gene, and the risk for dementia and related pathologies: The Honolulu-Asia Aging Study, *Diabetes 51*, 1256−1262.
27. Razay, G., and Wilcock, G. K. (1994) Hyperinsulinaemia and Alzheimer's disease, *Age Ageing 23*, 396−399.
28. Kuusisto, J., Koivisto, K., Mykkanen, L., Helkala, E. L., Vanhanen, M., Hanninen, T., Kervinen, K., Kesaniemi, Y. A., Riekkinen, P. J., and Laakso, M. (1997) Association between features of the insulin resistance syndrome and Alzheimer's disease independently of apolipoprotein E4 phenotype: Cross sectional population based study, *BMJ [Br. Med. J.] 315*, 1045−1049.
29. Arvanitakis, Z., Wilson, R. S., Bienias, J. L., Evans, D. A., and Bennett, D. A. (2004) Diabetes mellitus and risk of Alzheimer disease and decline in cognitive function, *Arch. Neurol. 61*, 661−666.
30. Kuo, W. L., Gehm, B. D., and Rosner, M. R. (1990) Cloning and expression of the cDNA for a *Drosophila* insulin-degrading enzyme, *Mol. Endocrinol. 4*, 1580−1591.
31. Baumeister, H., Muller, D., Rehbein, M., and Richter, D. (1993) The rat insulin-degrading enzyme. Molecular cloning and characterization of tissue-specific transcripts, *FEBS Lett. 317*, 250−254.
32. Kuo, W. L., Montag, A. G., and Rosner, M. R. (1993) Insulin-degrading enzyme is differentially expressed and developmentally regulated in various rat tissues, *Endocrinology 132*, 604−611.
33. Affholter, J. A., Fried, V. A., and Roth, R. A. (1988) Human insulin-degrading enzyme shares structural and functional homologies with *E. coli* protease III, *Science 242*, 1415−1418.
34. Ota, T., Suzuki, Y., Nishikawa, T., Otsuki, T., Sugiyama, T., Irie, R., Wakamatsu, A., Hayashi, K., Sato, H., Nagai, K., Kimura, K., Makita, H., Sekine, M., Obayashi, M., Nishi, T., Shibahara, T., Tanaka, T., Ishii, S., Yamamoto, J., Saito, K., Kawai, Y., Isono, Y., Nakamura, Y., Nagahari, K., Murakami, K., Yasuda, T., Iwayanagi, T., Wagatsuma, M., Shiratori, A., Sudo, H., Hosoiri, T., Kaku, Y., Kodaira, H., Kondo, H., Sugawara, M., Takahashi, M., Kanda, K., Yokoi, T., Furuya, T., Kikkawa, E., Omura, Y., Abe, K., Kamihara, K., Katsuta, N., Sato, K., Tanikawa, M., Yamazaki, M., Ninomiya, K., Ishibashi, T., Yamashita, H., Murakawa, K., Fujimori, K., Tanai, H., Kimata, M., Watanabe, M., Hiraoka, S., Chiba, Y., Ishida, S., Ono, Y., Takiguchi, S., Watanabe, S., Yosida, M., Hotuta, T., Kusano, J., Kanehori, K., Takahashi-Fujii, A., Hara, H., Tanase, T. O., Nomura, Y., Togiya, S., Komai, F., Hara, R., Takeuchi, K., Arita, M., Imose, N., Musashino, K., Yuuki, H., Oshima, A., Sasaki, N., Aotsuka, S., Yoshikawa, Y., Matsunawa, H., Ichihara, T., Shiohata, N., Sano, S., Moriya, S., Momiyama, H., Satoh, N., Takami, S., Terashima, Y., Suzuki, O., Nakagawa, S., Senoh, A., Mizoguchi, H., Goto, Y., Shimizu, F., Wakebe, H., Hishigaki, H., Watanabe, T., Sugiyama, A., et al. (2004) Complete sequencing and characterization of 21,243 full-length human cDNAs, *Nat. Genet. 36*, 40−45.
35. Vekrellis, K., Ye, Z., Qiu, W. Q., Walsh, D., Hartley, D., Chesneau, V., Rosner, M. R., and Selkoe, D. J. (2000) Neurons regulate extracellular levels of amyloid β-protein via proteolysis by insulin-degrading enzyme, *J. Neurosci. 20*, 1657−1665.
36. LaVoie, M. J., Fraering, P. C., Ostaszewski, B. L., Ye, W., Kimberly, W. T., Wolfe, M. S., and Selkoe, D. J. (2003) Assembly of the γ-secretase complex involves early formation of an intermediate subcomplex of Aph-1 and nicastrin, *J. Biol. Chem. 278*, 37213−37222.
37. Leissring, M. A., Lu, A., Condron, M. M., Teplow, D. B., Stein, R. L., Farris, W., and Selkoe, D. J. (2003) Kinetics of amyloid β-protein degradation determined by novel fluorescence- and fluorescence polarization-based assays, *J. Biol. Chem. 278*, 37314−37320.
38. Xia, W., Ray, W. J., Ostaszewski, B. L., Rahmati, T., Kimberly, W. T., Wolfe, M. S., Zhange, J., Goate, A. M., and Selkoe, D. J. (2000) Presenilin complexes with the C-terminal fragments of amyloid precursor protein at the sites of amyloid β-protein generation, *Proc. Natl. Acad. Sci. U.S.A. 97*, 9299−9304.
39. Gasteiger, E., Gattiker, A., Hoogland, C., Ivanyi, I., Appel, R. D., and Bairoch, A. (2003) ExPASy: The proteomics server for in-depth protein knowledge and analysis, *Nucleic Acids Res. 31*, 3784−3788.
40. Soltys, B. J., and Gupta, R. S. (1996) Immunoelectron microscopic localization of the 60-kDa heat shock chaperonin protein (Hsp60) in mammalian cells, *Exp. Cell Res. 222*, 16−27.
41. Kuo, W.-L., Gehm, B. D., Rosner, M. R., Li, W., and Keller, G. (1994) Inducible expression and cellular localization of insulin-degrading enzyme in a stably transfected cell line, *J. Biol. Chem. 269*, 22599−22606.
42. Song, E. S., Juliano, M. A., Juliano, L., and Hersh, L. B. (2003) Substrate activation of insulin-degrading enzyme (insulysin). A potential target for drug development, *J. Biol. Chem. 278*, 49789−49794.
43. Chesneau, V., and Rosner, M. R. (2000) Functional human insulin-degrading enzyme can be expressed in bacteria, *Protein Expression Purif. 19*, 91−98.
44. Lustbader, J. W., Cirilli, M., Lin, C., Xu, H. W., Takuma, K., Wang, N., Caspersen, C., Chen, X., Pollak, S., Chaney, M., Trinchese, F., Liu, S., Gunn-Moore, F., Lue, L. F., Walker, D. G., Kuppusamy, P., Zewier, Z. L., Arancio, O., Stern, D., Yan, S. S., and Wu, H. (2004) ABAD directly links Aβ to mitochondrial toxicity in Alzheimer's disease, *Science 304*, 448−452.
45. Conne, B., Stutz, A., and Vassalli, J. D. (2000) The 3′ untranslated region of messenger RNA: A molecular 'hotspot' for pathology? *Nat. Med. 6*, 637−641.
46. Hamel, F. G., Bennett, R. G., and Duckworth, W. C. (1998) Regulation of multicatalytic enzyme activity by insulin and the insulin-degrading enzyme, *Endocrinology 139*, 4061−4066.
47. Kupfer, S. R., Wilson, E. M., and French, F. S. (1994) Androgen and glucocorticoid receptors interact with insulin degrading enzyme, *J. Biol. Chem. 269*, 20622−20628.
48. Takai, D., and Jones, P. A. (2002) Comprehensive analysis of CpG islands in human chromosomes 21 and 22, *Proc. Natl. Acad. Sci. U.S.A. 99*, 3740−3745.
49. Authier, F., Bergeron, J. J., Ou, W. J., Rachubinski, R. A., Posner, B. I., and Walton, P. A. (1995) Degradation of the cleaved leader peptide of thiolase by a peroxisomal proteinase, *Proc. Natl. Acad. Sci. U.S.A. 92*, 3859−3863.
50. Schmitz, A., Schneider, A., Kummer, M. P., and Herzog, V. (2004) Endoplasmic reticulum-localized amyloid β-peptide is degraded in the cytosol by two distinct degradation pathways, *Traffic 5*, 89−101.
51. Ho, L., Qin, W., Pompl, P. N., Xiang, Z., Wang, J., Zhao, Z., Peng, Y., Cambareri, G., Rocher, A., Mobbs, C. V., Hof, P. R., and Pasinetti, G. M. (2004) Diet-induced insulin resistance promotes amyloidosis in a transgenic mouse model of Alzheimer's disease, *FASEB J. 18*, 902−904.
52. Cook, D. G., Leverenz, J. B., McMillan, P. J., Kulstad, J. J., Ericksen, S., Roth, R. A., Schellenberg, G. D., Jin, L. W., Kovacina, K. S., and Craft, S. (2003) Reduced hippocampal insulin-degrading enzyme in late-onset Alzheimer's disease is associated with the apolipoprotein E-ϵ4 allele, *Am. J. Pathol. 162*, 313−319.
53. Perez, A., Morelli, L., Cresto, J. C., and Castano, E. M. (2000) Degradation of soluble amyloid β-peptides 1−40, 1−42, and the Dutch variant 1−40Q by insulin degrading enzyme from Alzheimer disease and control brains, *Neurochem. Res. 25*, 247−255.

BI0476578